Analysis of the tuning and operation of reflection resonator EPR spectrometers

Vladimir Krymov[a,b] and Gary J. Gerfen[a,*]

[a] *Department of Physiology and Biophysics, Albert Einstein College of Medicine, Yeshiva University, 1300 Morris Park Avenue, Bronx, NY 10461, USA*
[b] *Donetsk Physical-Technical Institute, Ukrainian National Academy of Sciences, Donetsk, Ukraine*

Abstract

This paper investigates basic characteristics of the electron paramagnetic resonance (EPR) signal obtained from spectrometers employing reflection resonators. General equations are presented which reveal the phase and amplitude dependence on instrumental parameters of both components of the continuous wave (CW) EPR signal (absorption and dispersion). New phase vector diagrams derived from these general equations are presented for the analysis of the EPR response. The dependence of the phase and absolute value of the CW EPR signal on the local oscillator (LO) phase and on resonator offset and coupling is presented and analyzed. The EPR spectrometer tuning procedures for both balanced and unbalanced heterodyne receivers are analyzed in detail using the new phase diagrams. Extraneous signals at the RF input of the microwave receiver (resulting from circulator leakage and reflections in the resonator transmission line) have been taken into account and analyzed. It is shown that a final tuning condition that corresponds to an extremum of the receiver output as a function of the resonator frequency is necessary and sufficient for the acquisition of pure absorption signal. This condition is universal: it applies to all spectrometer configurations in all frequency ranges. High Frequency EPR spectrometer (130 GHz) data are used to generate experimental phase diagrams that illustrate the theoretical concepts presented in the paper. Conditions are presented under which the absorption signal can be measured with complete suppression of the dispersion, independent of the mutual frequency offset between the microwave source and the EPR sample resonator. Equations describing the approximate relationship between changes of the resonator properties (Q-factor and frequency) and paramagnetic susceptibility are derived and analyzed.
© 2003 Elsevier Science (USA). All rights reserved.

Keywords: Electron paramagnetic resonance; HF EPR; High frequency; Reflection coefficient; Microwave

1. Introduction

The basic principles describing instrumentation and sensitivity in EPR spectroscopy are well established and have been extensively discussed in several classic works [1–4]. However, these treatments emphasize the application of these principles primarily in the low frequency (LF) range. High frequency (90 GHz or greater) EPR spectroscopy (HF EPR) is now becoming an established and rapidly growing technique for the study of a variety of paramagnetic systems [5]. The smaller microwave wavelengths (and correspondingly smaller microwave spectrometer components) encountered in HF relative to LF EPR lead to instrumental characteristics which must be considered for proper tuning and operation of HF EPR spectrometers. The purpose of this work is to advance the theoretical framework within which the tuning and operation of reflection resonator EPR spectrometers of all the frequency bands can be accurately analyzed. The operation of these spectrometers is based on high Q-resonant structures that must be properly coupled to the microwave source in order to maximize sensitivity and stability.

General equations are presented that describe the tuning and matching of EPR resonators in all frequency ranges. These equations make clear the dependence of the EPR signal phase and amplitude on coupling and tuning parameters. From these equations, a graphical description of the resonator reflection coefficient (Γ) is

---

* Corresponding author. Fax: 1-718-430-8935.
E-mail address: gerfen@aecom.yu.edu (G.J. Gerfen).

developed to describe quantitatively the phenomenon of resonant tuning and matching. The reflection coefficient description is initially developed for the simple case of tuning and matching a basic resonant structure. The description is extended to include the phenomenon of resonant absorption/dispersion of microwave radiation by a sample, and the effects of the spectrometer receiver characteristics upon this magnetic resonance signal. Using this vector picture of the reflection coefficient description, a strategy is presented for the most effective means to tune and match microwave resonators. Through the analysis presented here, practical operational procedures are developed and evaluated with the intent of increasing signal-to-noise ratios and achieving a more complete separation of absorption and dispersion signals.

2. Resonator reflection coefficient

Spectrometers employing a reflection microwave resonator have generally proven to be more convenient and sensitive than those employing transmission probes, and are typically used when experimental circumstances allow. For a reflection resonator spectrometer, the EPR signal is detected by measuring variations in the microwave power reflected from the resonator as the sample absorbs or emits radiation upon achieving magnetic resonance. Thus, the resonator reflection coefficient Γ plays a central role in the analysis of EPR signal acquisition and spectrometer tuning.

It is well known that the resonator reflection coefficient can be represented by the following equation (for example, see [2, Eq. (3.7), p. 67]):

$$\Gamma = \frac{Z_{IN} - Z_0}{Z_{IN} + Z_0};\tag{1}$$

in which Γ is reflection coefficient, Z_{IN} is the resonator input impedance, and Z_0 is the transmission line characteristic impedance. The expression for the resonator input impedance Z_{IN} is also well known. Usually Z_{IN} is represented by means of the impedance of the EPR sample resonator equivalent series RLC circuit shown in Fig. 1 and Ref. (see [4, Eq. (10), p. 124]):

$$Z_{IN} = R_C + jX = R_C\left[1 + jQ_U\left(\frac{\omega}{\omega_0} - \frac{\omega_0}{\omega}\right)\right]$$

$$\approx R_C\left[1 + 2jQ_U\frac{\omega - \omega_0}{\omega_0}\right],\tag{2}$$

in which R_C is the equivalent resistance of the resonator, X is the equivalent reactive impedance of the resonator, ω is the microwave source angular frequency, ω_0 is the resonator resonant angular frequency, Q_U is the resonator unloaded Q-factor, and j is the imaginary unit. Eq. (2) utilizes the standard microwave frequency approximation of $(\omega_0 - \omega) \ll \omega$.

In general, the resonator Q-factor is defined as being proportional to the energy stored in the resonator and inversely proportional to the energy losses (see, for example, [2, p. 71] or [4, p. 125]). The unloaded Q-factor Q_U is inversely proportional to the sum of all the resonator stored energy losses with the exception of the coupling losses into the transmission line. These losses of the resonator stored energy into the transmission line are incorporated into the radiation Q-factor Q_R. Loaded Q-factor Q_L incorporates all the losses of the resonator stored energy, including the coupling losses into the transmission line, therefore $Q_L^{-1} = \left(Q_U^{-1} + Q_R^{-1}\right)$ in [2, Eq. (3.22), p. 72].

The absence of a transformer in Fig. 1 means that all microwave impedances are already transformed into a single RLC series circuit, i.e., the resonator impedances are transformed into the transmission line equivalent circuit, or the transmission line characteristic impedance is transformed into the resonator equivalent circuit: both of these situations are equivalent. Moreover, the ratio between impedances of the resonator and transmission line is determined by the coupling parameter and can be changed if coupling is variable. The substitution of Eq. (2) into (1) yields:

$$\Gamma \approx \left\{1 - \frac{Z_0}{R_C} + 2jQ_U\frac{\omega - \omega_0}{\omega_0}\right\}$$

$$\Big/ \left\{1 + \frac{Z_0}{R_C} + 2jQ_U\frac{\omega - \omega_0}{\omega_0}\right\}.\tag{3}$$

As it is evident from Fig. 1:

$$\frac{Z_0}{R_C} = \text{(Losses of the Resonator Stored Energy into the}$$

Transmission Line)/(Losses of the Resonator

$$\text{Stored Energy inside of the Resonator).}\tag{4}$$

Using the definitions of the Q-factors and coupling parameter β, Eq. (4) becomes (see [2, Eq. (3.23), p. 72]):

$$\frac{Z_0}{R_C} = \frac{\text{(Unloaded } Q\text{-factor)} = Q_U}{\text{(Radiation } Q\text{-factor)} = Q_R} = \frac{Q_U}{Q_R} = \beta.\tag{5}$$
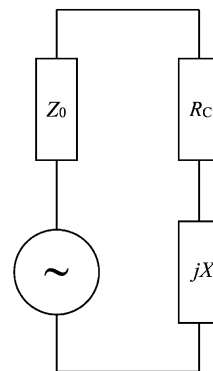

Fig. 1. Equivalent series RLC circuit representation of the EPR sample resonator. Z_0 is the transmission line characteristic impedance, R_C is the equivalent resistance of the resonator and X is the equivalent reactive impedance of the resonator.

Thus β is the coupling parameter of the resonator with the transmission line into which the resonator stored energy is being lost. The condition $\beta = 1$ is defined as critical coupling. It follows from Eqs. (3) and (5) that, when the resonator is tuned to its resonant frequency ($\omega = \omega_0$) and is matched to critical coupling, there is no reflected power, $Q_R = Q_U$ and $Q_L = 1/2\,Q_U$.

An important aspect of Eqs. (2) and (3) is the offset of the microwave frequency setting ω from the resonator frequency ω_0. A useful parameter for this analysis is provided by the normalized resonator offset ξ, defined as

$$\xi = -Q_U\left(\frac{\omega}{\omega_0} - \frac{\omega_0}{\omega}\right) \approx 2Q_U\frac{\omega_0 - \omega}{\omega_0}. \tag{6}$$

(A similar parameter a, equal to $-\xi/2$ and defined as a relative fractional detuning, is described in [6, p. 202].) Note that ξ and ω_0 are positively correlated (i.e., ξ is increasing when ω_0 is increasing) because we have defined ξ as the resonator normalized offset (as opposed to the microwave source offset). The reflection coefficient described by Eq. (3) can now be written

$$\Gamma = \frac{1 - \beta - j\xi}{1 + \beta - j\xi}. \tag{7}$$

Eq. (7) is valid for any value of the coupling parameter β and the normalized offset ξ. The utility of Eq. (7) derives from its independence from any resonator parameters except those which are varied in the tuning and matching process. Especially important is the lack of dependence on the resonator Q-factor, which allows a generalized analysis for any resonator.

The normalized offset values $\xi = \pm 1$ correspond to the offsets at the 50% levels of the resonator reflection dip in the small coupling limit. This is valid for any resonator with any unloaded Q-factor, and can be illustrated by calculating the values of the reflection coefficient for three values of ξ under conditions of $\beta \ll 1$ (i.e., small coupling):

$$\boxed{|\Gamma(\xi = 0)| = \frac{1-\beta}{1+\beta} \approx (1 - 2\beta),}$$

$$\boxed{|\Gamma(\xi = 1)| = \sqrt{\frac{(1-\beta)^2 + 1}{(1+\beta)^2 + 1}} \approx (1 - \beta),} \tag{8}$$

$$\boxed{|\Gamma(\xi = \pm\infty)| = 1.}$$

It follows that $|\Gamma(\xi = 1)| \approx (|\Gamma(\xi = 0)| + |\Gamma(\xi = \pm\infty)|)/2$: $\xi = 1$ corresponds to the offset $|\omega_0 - \omega|$ at which the reflection coefficient is at the 50% level of the resonator dip in the small coupling regime. These relations allow the angular frequency offset value $|\omega_0 - \omega|$ corresponding to the normalized offset value $|\xi| = 1$ to be expressed as a property of the unloaded Q-factor value. Defining $\Delta\omega_{0.5}$ as the absolute value of the offset $|\omega_0 - \omega|$ for $\xi = 1$ and inserting it and $\xi = 1$ into Eq. (6) yields an expression for the measurement of Q_U:

$$Q_U = \frac{\omega_0}{2(\Delta\omega_{0.5})}. \tag{9}$$

Note that this expression for Q_U differs by a factor of 2 in the denominator relative to that given by Poole [4, Eq. (11), p. 125] because $\Delta\omega_{0.5}$ is defined here as half of the value $\Delta\omega$ defined in [4]. The substitution of Eq. (9) into Eq. (6) gives the physical meaning of the normalized offset ξ:

$$\xi \approx \frac{\omega_0 - \omega}{\Delta\omega_{0.5}}, \tag{10}$$

i.e., the normalized offset ξ is equal to the ratio of absolute offset $\omega_0 - \omega$ over the resonator dip small-coupling half-width $\Delta\omega_{0.5}$. Note that in order to accurately measure the value of $2\Delta\omega_{0.5}$, one must adjust the resonator coupling to a small value and measure the width between the 50% levels of dip. However, for a given value of $\Delta\omega_{0.5}$, Eq. (10) is valid for $(\omega_0 - \omega) \ll \omega$ and all values of β.

It is well known that the tip of the vector representing the reflection coefficient Γ traces a circle in the phase plane when the resonator offset ξ is varied from $-\infty$ to $+\infty$ with $\beta = $ constant (see [2, Fig. 3.4, p. 68]). Therefore the Γ value from Eq. (7) can be separated into two components. The first component is dependent only on β, and the second is dependent on both variables, β and ξ, but its absolute value is independent of ξ. This partitioning of Γ yields (see Appendix A):
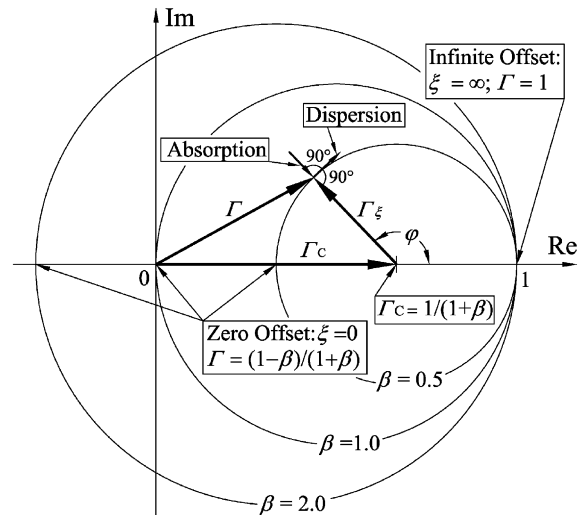
Fig. 2. Phase diagram of the EPR sample resonator reflection coefficient. The total reflection coefficient Γ consists of two components, Γ_C and Γ_ξ. The first component Γ_C is independent of the resonator offset ξ and therefore does not vary when the resonator frequency tuned. The absolute value of the second component Γ_ξ is also independent of ξ and therefore the tip of Γ_ξ describes a circle when the resonator frequency is tuned between $\xi = \pm\infty$. Three such circles are shown here for different values of the coupling parameter β: 0.5, 1.0, and 2.0. In addition, the phase directions of both components of the EPR signal (absorption and dispersion) are illustrated.

$$\boxed{\Gamma = \Gamma_C + \Gamma_\xi = \left(\frac{1}{1+\beta}\right) + \left(\frac{\beta}{1+\beta}\right)\exp j\varphi,}$$

$$\boxed{\Gamma_C = \left(\frac{1}{1+\beta}\right) \quad \Gamma_\xi = \left(\frac{\beta}{1+\beta}\right)\exp j\varphi,} \tag{11}$$

where

$$\varphi = \left[\pi + 2\tan^{-1}\left(\frac{\xi}{1+\beta}\right)\right]. \tag{12}$$

The phase diagram depicted in Fig. 2 provides a graphical representation of the resonator reflection coefficient components from Eqs. (11) and (12) for $\beta = 0.5$ as the resonator offset ξ is varied between $-\infty$ and $+\infty$. Γ_C is defined solely by β while the tip of Γ_ξ traces a circle defined by $\varphi(\xi,\beta)$ as the offset ξ is varied. Also shown are two circles defined by the tip of Γ_ξ for $\beta = 1.0$ and $\beta = 2.0$. Note that the phase angle $\varphi = \pm 90°$ when $\xi = \pm(1+\beta)$.

Phase diagrams of the resonator reflection coefficient (depicted in Fig. 2 and subsequently in Figs. 5–7) are very convenient for characterization and tuning of reflection resonators. They are similar to Smith Charts (for example, see [7, Section 12.9]), but describe more directly the features important for magnetic resonance spectrometers, as discussed in Appendix B.

3. CW EPR signal as a change in the resonator reflection coefficient

In order to utilize the phase vector diagrams for analysis of spectrometer characteristics, it is necessary to incorporate the CW EPR signal. As the magnetic resonance condition is achieved in EPR instruments utilizing reflection resonators, changes of the sample paramagnetic susceptibility χ lead to variation in the resonator reflection coefficient. This variation in Γ is detected by the spectrometer receiver to produce the CW EPR signal. The total paramagnetic susceptibility χ is a complex quantity $\chi = (\chi' - j\chi'')$. The real component χ' causes variation of the resonator frequency ω_0 which leads to the dispersion CW EPR signal, and the imaginary component χ'' causes variation of the unloaded Q-factor Q_U which leads to the absorption signal. Using Eqs. (5)–(7), it is possible to determine the change in the reflection coefficient ($\Delta\Gamma$) as a function of the change in unloaded resonator quality factor and resonance offset (ΔQ_U and $\Delta\xi$, respectively):

$$\Delta\Gamma = \frac{-2\beta}{(1+\beta-j\xi)^2}\left(\frac{\Delta Q_U}{Q_U} + j\Delta\xi\right). \tag{13}$$

$\Delta\xi$ is defined as originating only from the resonator frequency change ($\Delta\omega_0$) and not from a change of the resonator Q-factor Q_U, i.e., $\Delta\xi$ is the change in ξ as a function of ω_0 and thus according to Eq. (10)

$\Delta\xi = \{\Delta\omega_0/\Delta\omega_{0.5}\}$. Eq. (13) is valid for small changes such that $|\Delta Q_U/Q_U| \ll 1, |\Delta\xi| \ll 1$ and therefore $|\Delta\Gamma| \ll 1$. For small values of paramagnetic susceptibility, i.e., when $|\chi' - j\chi''| \ll 1$, it is shown in Appendix C that this relationship between paramagnetic susceptibility and ΔQ_U and $\Delta\xi$ can be described by:

$$\left(\frac{\Delta Q_U}{Q_U} + j\Delta\xi\right) = -Q_U\eta(\chi'' + j\chi') \tag{14}$$

in which η is the filling factor of the EPR sample in the resonator by the magnetic field energy:

$$\eta = \frac{\int_{Sample} \mathbf{H}_1^* \cdot \mathbf{H}_1 \sin^2\phi\, dV}{\int_{Resonator} \mathbf{H}_1^* \cdot \mathbf{H}_1\, dV}, \tag{15}$$

$\mathbf{H}_1$ is amplitude of the microwave magnetic field; ϕ is angle between $\mathbf{H}_1$ and the static magnetic field $\mathbf{H}_0$.

Substitution of Eq. (14) into Eq. (13) gives the relationship between the reflection coefficient variation $\Delta\Gamma_\chi$ and the paramagnetic susceptibility ($\chi' - j\chi''$):

$$\Delta\Gamma_\chi = \frac{2\beta}{(1+\beta-j\xi)^2}Q_U\eta(\chi'' + j\chi') \tag{16}$$

or

$$\boxed{\Delta\Gamma_\chi = (\chi'' + j\chi')(Q_U\eta)\left(\frac{2\beta}{(1+\beta)^2 + \xi^2}\right)\exp j(\varphi - \pi)}$$

$$\boxed{\Gamma_\xi = \left(\frac{\beta}{1+\beta}\right)\exp j\varphi,} \tag{17}$$

in which φ is defined in Eq. (12). Γ_ξ (from Eq. (11)) has been rewritten in Eq. (17) to facilitate comparison. It is evident from Eq. (17) that the *EPR absorption signal (which is proportional to χ'') is always antiparallel to Γ_ξ, and the EPR dispersion signal (which is proportional to χ') is always orthogonal to Γ_ξ*. This is an important result which always allows the exact tuning of the EPR signal phase based on the phase of Γ_ξ even if an EPR signal cannot be readily observed (as may be the case for weak signals requiring extensive signal averaging). Both the absorption and dispersion components of the EPR signal are shown in Fig. 2.

It follows from Eq. (17) that the EPR signal magnitude $|\Delta\Gamma_\chi|$ is maximal when $\beta = 1$ and $\xi = 0$. However, it is evident from Fig. 3a that this maximum is relatively broad. The solid traces in Fig. 3a show the EPR signal relative magnitude as a function of normalized offset ξ for several constant values of β. The dashed trace corresponds to the variable $\beta = \sqrt{1 + \xi^2}$, at which the EPR signal is maximized for every value of ξ. This optimization allows the determination of the optimal coupling for a given frequency offset, which may be useful for the implementation of multifrequency ELDOR experiments. Fig. 3b presents the phase of the EPR absorption signal as a function of ξ for several values of β (the EPR dispersion signal phase traces are equal to the absorption traces shifted by 90° and those of the reflection coefficient component Γ_ξ are shifted by 180°).
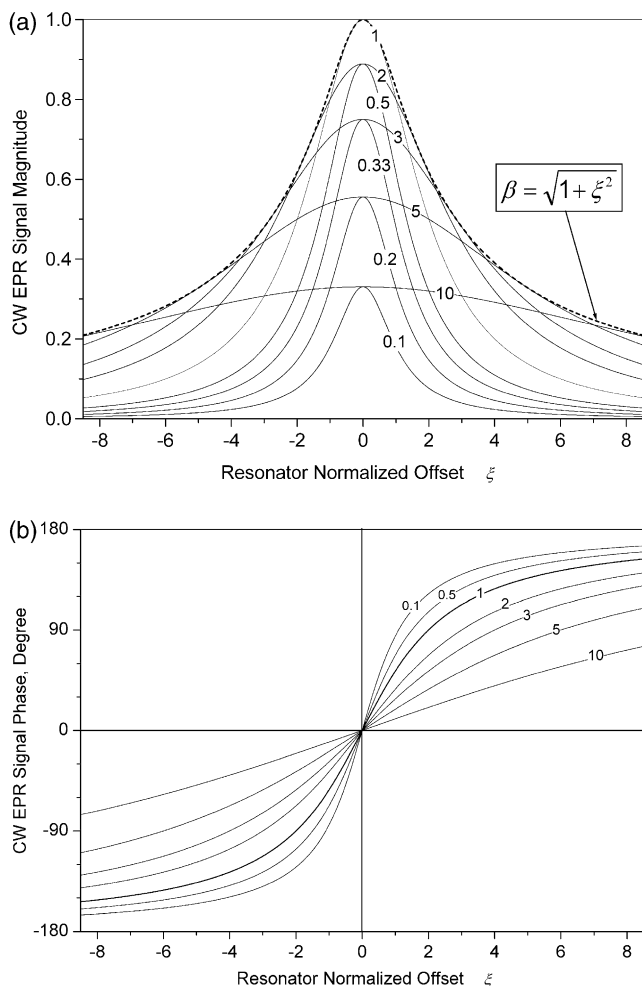
Fig. 3. CW EPR signal magnitude (a) and phase (b) as functions of the resonator normalized offset ξ for selected values of the resonator coupling parameter β. The dashed trace in (a) corresponds to the function $\beta = \sqrt{1 + \xi^2}$ which maximizes the signal for every value of ξ. The appropriate value of β used to generate each solid trace is indicated.

Fig. 3a illustrates that precise tuning of the resonator frequency and coupling parameter is not crucial for achieving adequate signal *intensity*. However, the quality of EPR spectra depends on additional factors that are strongly influenced by EPR resonator tuning. The precise tuning of the resonator frequency is necessary to obtain the correct shape of the CW EPR signal. Also precise tuning of both the resonator frequency and coupling parameter may be required to minimize the microwave source noise contribution to total noise of the EPR signal receiver if the source noise is significant.

4. Application of the phase diagram analysis to spectrometer tuning

The phase diagrams developed in the preceding sections can be used to optimize the tuning procedures of

reflection resonator CW EPR spectrometers. Steps such as setting the LO phase, the resonator frequency and its coupling to the transmission line can be evaluated and their effects on the EPR signal predicted. The analysis is based on Eqs. (11), (12), (17), which represent the microwave signal. Fig. 4 illustrates the basic components of the EPR spectrometer that are relevant for our analysis of microwave tuning. The resonator containing the EPR sample is connected to the microwave source and receiver by means of a circulator. The phase between the signal power P_3 (RF) and Local Oscillator (LO) can be set by a phase shifter. Fig. 4 is appropriate for both heterodyne microwave receivers, in which the LO and RF frequencies are not equal, and homodyne receivers, in which the LO and RF frequencies are equal and generated by the same source or locked to the same master oscillator.

The present analysis will be carried out for two types of the receivers—balanced and unbalanced. The main advantage obtained from the balanced receiver is a rejection of the signal from the LO, which is important when the LO noise is dominant and must be suppressed. It is assumed in the subsequent analysis that the output DC signal of the balanced receiver contains the RF input signal only and the LO signal is suppressed completely, and that the output DC signal of the unbalanced receiver consists of both the RF and LO signals. Because unbalanced receivers are typically constructed using single-ended mixers, which have only one input for both RF and LO signals, the same gain and losses apply to the RF and LO signals. Utilization of an unbalanced receiver is acceptable when the LO does not introduce significant noise into the receiver.

In the following analysis, particular attention is given to the proper phasing of the EPR signal. Issues regarding the EPR signal phase have been previously investigated and typically can be addressed in a straightforward fashion at low frequency [2,8]. However, as will be discussed, extending EPR spectroscopy

Fig. 4. Simplified block diagram of an EPR spectrometer employing a heterodyne or homodyne receiver and a reflection resonator.

to high frequencies introduces additional complications and motivates further consideration of this issue.

4.1. Balanced receiver

The output signal of the balanced receiver is proportional to the microwave signal at the receiver RF input and is dependent on the phase between the RF and the LO signals. Phase diagrams for a spectrometer using a balanced receive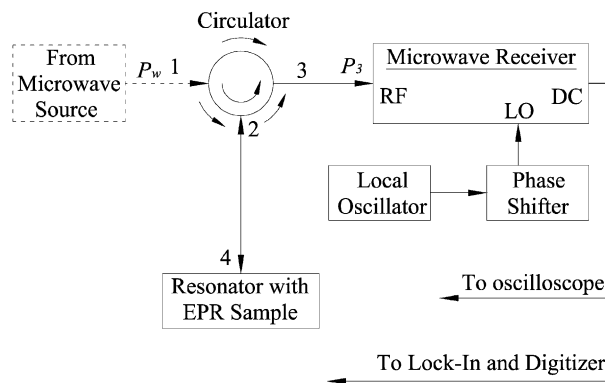r are shown in Fig. 5a (undercoupling case) and Fig. 5b (overcoupling case). The balanced receiver detects the inphase/antiphase component of the RF input but does not detect its orthogonal component. In other words, the balanced receiver detects the pro-

Fig. 5. Phase diagrams for an EPR spectrometer employing a balanced receiver. Phase diagrams of the EPR sample resonator reflection coefficient $\Gamma = (\Gamma_C + \Gamma_\xi)$ and both components of the EPR signal (absorption and dispersion), as well as their projections on the LO phase direction, are illustrated. The situations for undercoupling ($\beta < 1$) and overcoupling ($\beta > 1$) are shown in Fig. 5a and b, respectively. The LO phase setting has been chosen arbitrarily. The spectrometer has been exactly tuned for the acquisition of pure absorption signal in both diagrams.

jection of the RF phase vector onto the LO phase vector. Therefore the DC output signal of the receiver is proportional to the projection of the RF input signal (the signal at point 3 in Fig. 4) on the LO phase direction. That projection is equal to $|\Gamma| \sin \psi$ in which the angle ψ is a function of both φ (as determined by the resonant offset ξ) and the phase of the LO (defined as α). The phase shifter in Fig. 4 controls the value of α and thus controls the magnitude and polarity of the receiver DC output.

The diagrams depicted in Figs. 5a and b correspond to the spectrometer tuned exactly to the absorption signal for the general case of an arbitrary phasing between the RF and LO (i.e., $\alpha \neq 0°$ or $180°$). The arbitrary phase of α in Fig. 5 illustrates that pure absorption can be obtained regardless of the phase of the LO (see below). However, the EPR signal is not maximized in this tuned state with $\alpha \neq 0°$ or $180°$ because $\xi \neq 0$ (see Fig. 3a).

The initial tuning steps involve phasing the LO properly by setting $\alpha = 0°$ or $180°$ with respect to the reflected microwaves from the resonator. In order to achieve this value of α, the LO phasing must be done at infinite resonance offset, i.e., making $\xi = \pm\infty$ by tuning the resonator well off resonance and thus aligning Γ along the real axis. Step 1 is thus adjusting the resonance of the resonator to infinite offset. Under this condition, as the phase shifter is varied in step 2 of the tuning process, the DC output of the receiver will cyclically vary from a maximum value ($\alpha = 0°$), through 0 ($\alpha = 90°$), to a minimum value ($\alpha = 180°$). The correct phasing ($\alpha = 0°$ or $180°$) corresponds to the maximum or minimum of the receiver output.

The next step in the process is tuning the EPR resonator to its resonance frequency, i.e., setting $\xi = 0$. As is seen from Figs. 5a and b, complete separation of the absorption and dispersion signals is achieved when collinearity of the phase vectors Γ_ξ and LO is reached. This condition of collinearity corresponds to the minimum or maximum of the receiver DC output. Both conditions (zero offset ($\xi = 0$) and collinearity of Γ_ξ and LO) can be achieved simultaneously only if α has been tuned to $0°$ or $180°$ in the previous tuning step. At this stage, the LO phase and resonator offset have been set, but the coupling has not yet been tuned to critical ($\beta = 1$), at which the EPR signal is a maximum (Fig. 3a). Clearly the coupling can be tuned only when the resonator is on resonance ($\xi = 0$), but the resonator frequency must be the final act of spectrometer tuning in order to achieve the maximal collinearity of Γ_ξ and LO and thus the best separation of the absorption and dispersion signals at the receiver output. Therefore the final stage of the tuning process must be the alternate trims of frequency and coupling, and the final act must be the trim of the resonance frequency. The correct tuning point is always at an extreme of the receiver output

signal. There are two extrema when the offset ξ is tuned to $\pm\infty$: one is a maximum, the other a minimum. It is evident from Figs. 5a and b that more intense extremum has a smaller offset ξ and therefore produces a more intense EPR signal.

The pure dispersion signal can be detected by shifting the LO phase by 90° after final tuning to the pure adsorption signal. Receivers with two outputs in quadrature are preferred because they measure both the absorption and dispersion signal components simultaneously.

Figs. 5a and b, which depict the exact tuning to pure absorption at $\alpha \neq 0°$ or 180°, illustrate that even a spectrometer with an arbitrarily set LO phase can be tuned to achieve complete separation of absorption and dispersion signals by means of the observation of the resonator reflection only, independent of the receiver phase. *The final tuning condition, which corresponds to an extremum of the receiver output as a function of the resonator frequency, is necessary and sufficient for the acquisition of pure absorption signal.* The tuning process does not require the EPR signal itself, which may be too weak to observe without extensive averaging. Moreover, sweeping of the microwave frequency is not necessary for the correct matching of the resonator or phasing of the EPR signal.

4.2. Unbalanced receiver

The output signal of the unbalanced receiver is proportional to the combined microwave power of both the RF and LO signals. Phase diagrams appropriate for an unbalanced receiver are shown in Figs. 6a and b. Both figures depict an untuned, overcoupled resonator with the LO phase arbitrarily set such that $\alpha \neq 0°$ or 180°. R is the normalized LO phase vector. The normalization of R is achieved by dividing the LO phase vector magnitude at the receiver output by the RF signal magnitude at infinite resonator frequency offset ($\xi = \pm\infty$), also at the receiver output. The phase vector $G = R + \Gamma$ is the total input microwave signal of the unbalanced receiver, and therefore the DC signal at the receiver output is proportional to $|G|$.

Tuning for the case of an unbalanced receiver is equivalent to that described for a balanced receiver. The first step is to offset the resonance of the resonator so that the phase of R can be made collinear with $\Gamma(\xi = \pm\infty)$ ($\alpha = 0°$ or 180°). The correct phasing corresponds to the DC extreme at the output of the receiver when the total microwave signal $|G|$ is at its extreme. The magnitude of the receiver output is maximal when the phases of R and of $\Gamma(\xi = \pm\infty)$ are equal (i.e., when phase vectors R and $\Gamma(\xi = \pm\infty)$ are parallel and $\alpha = 0°$), and it is minimal when phases of R and of $\Gamma(\xi = \pm\infty)$ are shifted by 180° (i.e., when phase vectors R and $\Gamma(\xi = \pm\infty)$ are antiparallel and $\alpha = \pm180°$).
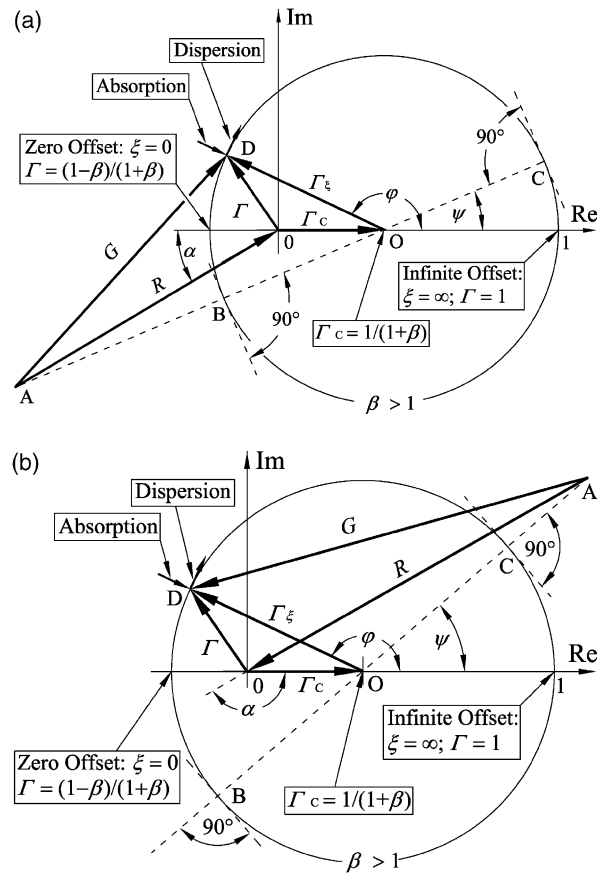

Fig. 6. Phase diagrams for an EPR spectrometer employing an unbalanced receiver. Phase diagrams of the reflection coefficient $\Gamma = (\Gamma_C + \Gamma_\xi)$ and of both components of the EPR signal (absorption and dispersion) are illustrated for the case of an overcoupled resonator. R, which is the LO phase vector normalized to $|\Gamma|$, is shifted by 180° in Fig. 6b relative to Fig. 6a. The output DC signal is proportional to $|G| = |R + \Gamma|$. The LO phase setting has been chosen arbitrarily. The spectrometer will be exactly tuned to the absorption signal when point D is coincident with points B or C. Those tuning points correspond to extrema of the receiver output DC signal.

Again, the tuning of the resonator frequency must be the final step of the tuning process in order to achieve correct phasing of the EPR signal. It is evident from Figs. 6a and b that collinearity of the phase vectors Γ_ξ and G provides a pure absorptive EPR signal and that this condition is reached at the extrema of $|G|$. Thus the resonance frequency offset of the resonator ξ is varied to minimize or maximize the output of the receiver. For the case in which α has been set to 0° or 180°, this minimization/maximization corresponds to $\xi = 0$.

Figs. 6a and b correspond to two cases in which $\alpha \neq 0°$ or 180°, with the phase of R in Fig. 6b shifted by 180° compared to that in Fig. 6a. These cases have been presented to illustrate that proper phasing can be achieved even with an arbitrary LO phase setting in a spectrometer with an unbalanced receiver, as has been demonstrated for the case of a balanced receiver (Fig. 5a and b). The spectrometer is correctly tuned when the

resonator offset is varied such that point D (the tip of Γ_ξ) becomes coincident with points B or C. This corresponds to the extrema of $|G|$, and ensures the correct phasing such that the in-phase receiver signal consists of 100% absorption and 0% dispersion. An extremum of $|G| = |R + \Gamma|$ corresponds to an extremum of the receiver output. Placement of point D at point B or point C each results in an extremum of $|G|$. One placement is a maximum of $|G|$ (point C in Fig. 6a and point B in Fig. 6b); the other corresponds to a minimum (point B in Fig. 6a and C in Fig. 6b). It is clear from Fig. 6a and b that the more intense extreme has a lower ξ offset and therefore a more intense EPR signal. Thus point B is the correct tuning position in both Fig. 6a and b.

During the tuning process, whether the extremum of $|G|$ and thus receiver output signal extremum is a maximum or a minimum depends on the phase and magnitude of R. However, there is a single tuning state in which no extrema of $|G|$ exist: when points A and O are coincident, i.e., when $R = -\Gamma_C$. When this condition is met, $G = \Gamma_\xi$ and varying ξ changes the phase, but not the magnitude, of G. This is an interesting condition because it results in a constant magnitude of the receiver output signal regardless of resonator frequency offset. Thus, if an unbalanced receiver is used and $R = -\Gamma_C$, no resonator dip will be observable. In addition, the EPR signal is pure absorption regardless of the resonator frequency offset, and no dispersion will be admixed. This characteristic may be useful for experiments that involve a high degree of microphonics, such as low temperature experiments with boiling cryogens or in vivo experiments with shifting animals. Such suppression of the dispersion signal at the condition of $R = -\Gamma_C$ was described previously in [2, pp. 186–187, Eq. (6.19), and Fig. 6.7] using a different formalism and phase vector representation.

After tuning to the pure absorption signal, switching the detection to pure dispersion signal in a spectrometer with an unbalanced receiver is not trivial. It is possible to measure the dispersion signal by shifting the phase of the LO (and thus R) by 90° after the resonator frequency has been tuned to pure absorption only if $|\Gamma| \ll |R|$. However, if $|\Gamma|$ and $|R|$ are comparable, setting the phase shift of the LO to detect pure dispersion will be extremely difficult because the correct value will not be constant but will be dependent on the tuning. Clearly the ideal experimental configuration with respect to phase is to employ a balanced receiver with outputs in quadrature.

4.3. Balanced receiver with extraneous signals at the RF input

The analysis presented in Section 4.1 corresponds to the ideal case of the receiver RF input power consisting of only the reflection from the resonator with an EPR

sample. In reality, power P_w also enters the receiver as a result of circulator leakage and transmission line reflections between the circulator and resonator with the EPR sample, i.e., between points 2 and 4 of Fig. 4. The circulator leakage results from the direct transmission of the microwave power from point 1 to point 3. Reflections can be generated by any discontinuity or imperfection in the transmission line or waveguide, the most common being flange connections. In the following discussion, any extraneous power at the receiver RF input not originating from the EPR sample resonator will be defined as leakage power.

As is true for the ideal case of no leakage power, the tuning procedures for a balanced receiver with leakage power is the same for both overcoupled and undercoupled resonators. The phase diagram, shown in Fig. 7, represents an EPR spectrometer with a balanced receiver and an overcoupled resonator and is therefore similar to that presented in Fig. 5b. The only difference is an additional vector L in Fig. 7 which represents the leakage power. The leakage phase vector L is normalized in the same manner as the LO phase vector R in the unbalanced receiver (see above and Fig. 6). The phase vector $N = L + \Gamma$ is the total microwave signal at the receiver input (point 3 in Fig. 4). The angle γ in Fig. 7 is

Fig. 7. Phase diagram for an EPR spectrometer with a balanced receiver in the presence of an extraneous coherent signal at the receiver RF input. Phase diagrams of the EPR sample resonator reflection coefficient $\Gamma = (\Gamma_C + \Gamma_\xi)$, the extraneous signal L and both components of the EPR signal (absorption and dispersion) are shown for an overcoupled resonator. Projections of $N = (\Gamma + L)$ and of the EPR signal onto the LO phase direction are also illustrated. Phases of the LO and of the leakage L have been chosen arbitrarily. The spectrometer is exactly tuned for acquisition of the pure absorption signal. Dash-dotted vector $N(\xi = \infty)$ corresponds to the infinite offset such that $\xi = \pm\infty$.

the phase angle between the leakage L and the reflection coefficient at infinite resonator offset $\Gamma(\xi = \pm\infty)$.

Fig. 7 corresponds to a spectrometer tuned to pure absorption signal for the case of arbitrarily set phases of both the leakage L and LO. Tuning with arbitrary L vector and LO phasing illustrates the general principle that the pure absorption or dispersion spectrum can be obtained simply by means of tuning the resonator frequency, regardless of the relative phase of the LO and the RF signals or the presence of any extraneous coherent signals on the receiver RF input.

The procedure for achieving the correctly tuned state of a spectrometer under actual conditions (i.e., with leakage power) is the same as previously described without leakage power. This applies for spectrometers with either balanced or unbalanced receivers. However, there is one difference in the final condition of the tuned states with and without arbitrarily phased leakage power: $\alpha = 0°$ or 180° without leakage power but $\alpha' = 0°$ or 180° with leakage power. The vector $N(\xi = \infty)$, connecting points A and B in Fig. 7, can be used to illustrate this. $N(\xi = \infty)$ is the total microwave signal at the receiver RF input when the resonator is offset to infinity. The initial tuning steps (i.e., phasing the LO with an offset resonator) lead to the LO phase direction collinear to vector $N(\xi = \infty)$: this sets $\alpha' = 0°$ or 180°. The equivalent condition with no leakage ($\alpha = 0°$ or 180°) is preferable because the sensitivity to the microwave source phase noise is minimal in this case. In order to achieve the tuning state with $\alpha' = \alpha = 0°$ or 180°, first the leakage vector L must be phased such that $\gamma = 0°$ or 180°. This can be done by use of a phase shifter inserted between the circulator and the resonator (i.e., between points 2 and 4 in Fig. 4).

5. Experimental results

The phase diagrams described above can be generated experimentally and used to analyze and tune an EPR spectrometer equipped with a microwave receiver with two outputs in quadrature. One simply connects the two receiver outputs to an oscilloscope set to the XY display mode. Tuning the resonator through its frequency range, between the upper and lower limits, will describe a circle on the oscilloscope screen corresponding to the circles presented in the phase diagrams. An example of such a circle, measured using an overcoupled H_{011}-mode cylindrical resonator on a 130-GHz EPR spectrometer, is shown in the Fig. 8. Values along the orthogonal axes "Output X" and "Output Y" are proportional to the two orthogonal output signals of the spectrometer receiver. Of the theoretical curves presented in this paper, Fig. 7 is the most applicable for the description of the experimental data in Fig. 8. The axis "Output X" is defined as parallel to Local Oscillator
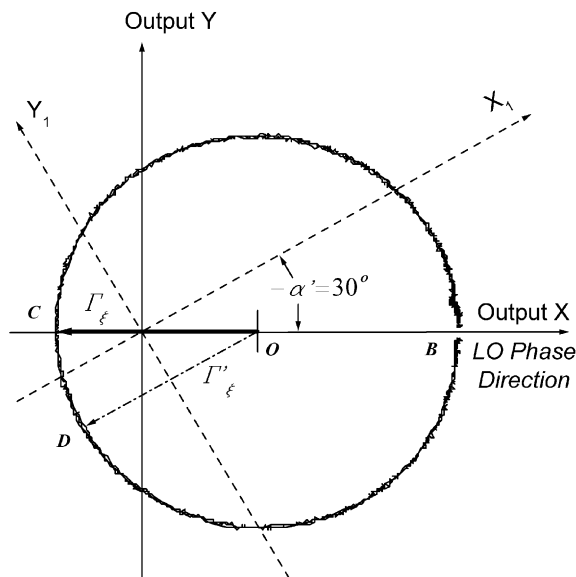
Fig. 8. Phase diagram of the resonator reflection coefficient measured using a 130-GHz EPR spectrometer with a balanced receiver and two outputs in quadrature. Outputs X and Y are represented as the abscissa and ordinate, respectively. Point B corresponds to an infinite resonator offset. Point C and vector Γ_ξ correspond to exact tuning of the resonator with the LO phased parallel to X. The two orthogonal dashed axes X_1 and Y_1 correspond to the LO phase direction $\alpha' = -30°$. The dash-dotted vector Γ'_ξ and point D correspond to the exact tuning of the resonator to pure absorption/dispersion at this value of α'.

phase direction in Fig. 7. For the generation of Fig. 8, the local oscillator has been phased using the tuning procedures described above such that the phase vector $N(\xi = \infty)$ from Fig. 7 is set parallel with axis "Output X" (i.e., to $\alpha' = 0°$). Point B in Fig. 8 corresponds to an infinite resonator offset that cannot be physically achieved: the measured circle cannot attain this point and therefore a small break occurs. The symmetry of the measured circle relative the axis "Output X" in Fig. 8 indicates that vectors L and $N(\xi = \infty)$ from Fig. 7 are parallel (and therefore $\gamma = 0°$). Point O in Fig. 8 is the origin of the circle, and point C and vector Γ_ξ correspond to exact tuning of the resonator. The two orthogonal dashed axes X_1 and Y_1 correspond to the LO phase direction phasing $\alpha' = -30°$. The dash-dotted vector Γ'_ξ and point D corresponds to the exact tuning the resonator to pure absorption/dispersion at this value of α'.

Fig. 9 presents CW EPR spectra, measured with an overcoupled H_{011}-mode cylindrical resonator at 130-GHz, that consist of both the absorption and dispersion signals of one of the six Mn(II) hyperfine lines from a powder of Mn^{2+} doped into MgO. First harmonics of both the absorption (solid traces) and dispersion (dashed traces) CW EPR spectra are represented on the left (Fig. 9a, c, and e). On the right (Fig. 9b, d, and f) are the corresponding phase vector diagrams of the signals. The horizontal (Output X) and vertical axis (Output Y)
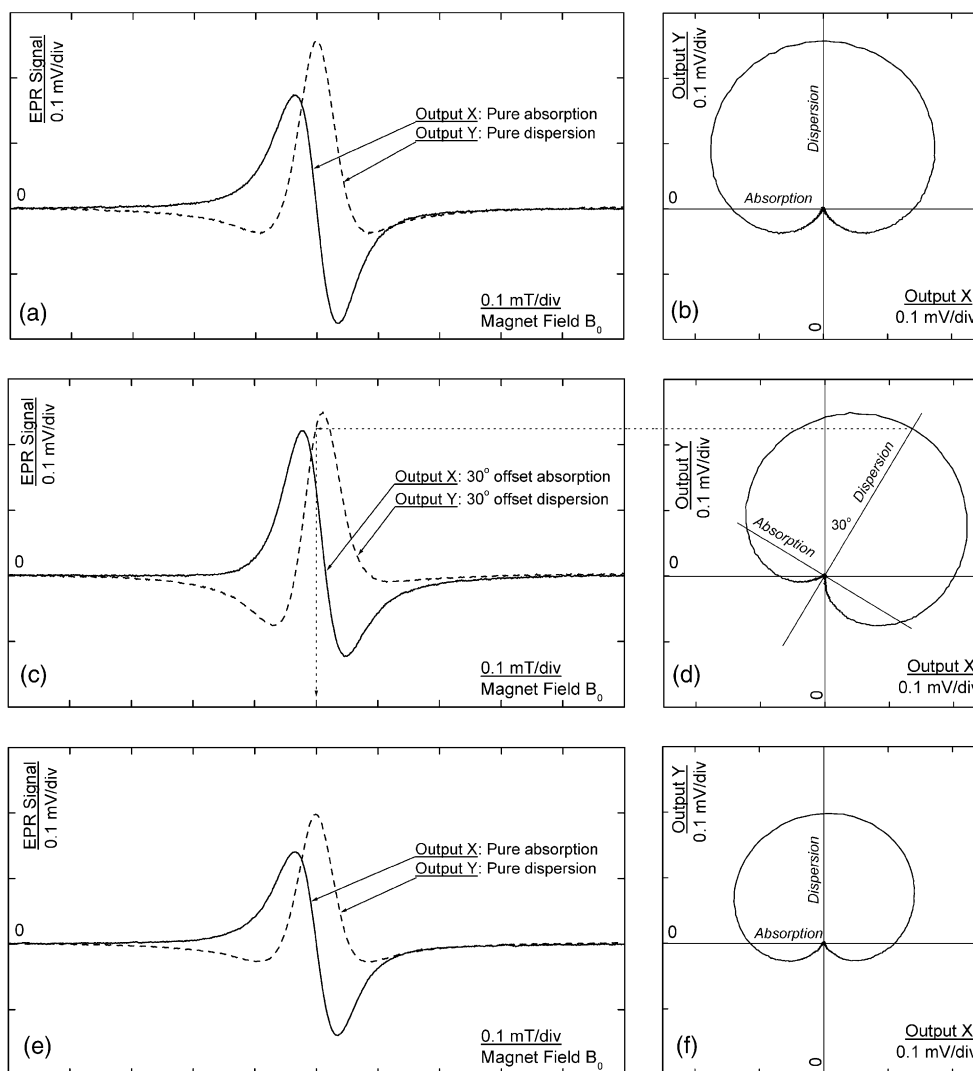
Fig. 9. CW EPR spectra (130 GHz) of one of the six Mn(II) hyperfine lines from a powder of Mn^{2+} doped into MgO. Absorption (solid) and dispersion (dashed) of the same hyperfine line are presented in A, C, and E. The phase diagram corresponding to each spectrum is shown to the right, in B, D, and F, respectively. The values of the abscissa and ordinate of the phase diagrams are equal to the values of the absorption and dispersion, respectively. Spectrum A and phase diagram B were acquired after proper spectrometer tuning as described in Section 4. Next, the receiver phase was offset by $-30°$ and spectrum C and phase diagram D were acquired. Finally, keeping this $-30°$ phase offset, the resonator frequency was tuned to the minimum signal at the receiver Output X and spectrum E and phase diagram F were acquired. All measurements were made with an overcoupled H_{011}-mode cylindrical resonator on the same sample. Experimental parameters were as follows: Spin concentration, approximately $1–2 \times 10^{-5}$ mol/liter; temperature, 293 K; resonator-filling factor, ~0.05; microwave power at the coupling hole of the EPR sample resonator, ~3 μW; field modulation, ~0.05 mT peak-to-peak; B_0 window, 1 mT; B_0 ramp rate, 0.1 mT/s; time constant, 30 ms.

values of the phase diagrams are proportional to the EPR first harmonic absorption and dispersion signals, respectively.

Fig. 9a and b display the spectrum and phase diagram measured with the resonator tuned to point C (Fig. 8) and the LO phase set such that $\alpha' = 0°$ (Figs. 7 and 8). The tuning procedure, executed as described in Section 4.3, results in complete separation of the absorption and dispersion signals. Figs. 9c and d were measured after the LO phase was rotated by 30° such that $\alpha' = -30°$, with all other parameters identical to a and b, (including the resonator left in point C of Fig. 8). The spectra in 9c

are now admixtures of absorption and dispersion, and Fig. 9d illustrates that the EPR signal phase diagram was rotated by the same angle of 30° relative to 9b. The third spectrum, corresponding to Fig. 9e and f, was measured after tuning the resonator frequency to the minimum signal at the receiver Output X (i.e., to point D in Fig. 8), without a change of the LO phase as set in Fig. 9c and d (i.e., with $\alpha' = -30°$). Fig. 9e again shows the complete separation of absorption and dispersion, as in Fig. 9a. It is also evident that the EPR signal phase diagram Fig. 9f has been rotated back to state of shown in Fig. 9b. However, the amplitude of 9e is smaller

because the slight resonator frequency offset from the microwave source produces a smaller signal (Fig. 3a).

Fig. 9 demonstrates experimentally that the correct phasing of the EPR signal can be achieved without a preliminary adjustment of the EPR signal phase, simply by the accurate tuning of the resonator frequency. Of course, the correct signal phase can also be achieved by tuning the microwave source frequency to the resonator frequency: instrumental characteristics at low frequencies permit this to be the standard tuning procedure in X and Q band EPR. However, at high frequencies this procedure may be problematic. Moreover, stable high frequency sources are not easily tunable, so HF spectrometers often use tunable resonators and fixed frequency sources. Phasing can also be achieved directly by observing the EPR signal itself and adjusting the LO phase to achieve complete separation of absorption and dispersion, but this is not possible for samples with very weak signal intensities that may require averaging to observe. The resonator frequency tuning procedure as described in Section 4 can be used to achieve the correct phasing, without the need to observe the EPR signal. As is evident from the phase diagrams (Figs. 5–7), the pure absorption signal is always acquired when the receiver output is set to an extremum as a function of the resonator frequency: this condition is necessary and sufficient for the acquisition of pure absorption signal.

The experimental phase diagrams shown Fig. 9 were obtained from a simple single line EPR spectrum and serve to illustrate the principles and equations presented in this paper. Phase diagrams derived from broad, multiline spectra are much more complicated and thus the general practicality of the diagrams is limited. However, when studying samples with well characterized lineshapes (such as nitroxides), these CW EPR phase diagrams may be useful for addressing the following issues. (1) Precise determination of the EPR spectra field position when both measured orthogonal signals are mixtures of absorption and dispersion. This technique is illustrated by the dotted lines in Fig. 9c and d. (2) Simple determination of the EPR signal phase when both measured orthogonal signals are mixtures of absorption and dispersion. Changing the EPR signal phase by a given angle does not change the EPR phase diagram shape but only rotates it by that same angle. This rotation is evident from a comparison of Fig. 9b and d. (3) Determination of spectral distortion caused by a strong EPR signal. It is well known that a very intense EPR signal can lead to spectral distortion. This distortion is caused by a large variation in the mean values of both the EPR resonator frequency and Q-factor as the magnetic field is swept through resonance. Spectral distortion can be characterized by the comparison of spectra measured with different tuned states of the EPR resonator frequency. For example, one spectrum can be measured with zero offset (i.e., with $\xi = 0$) and another with a small offset of $\xi \approx 0.5 - 1$. The shape of the phase diagrams will be different for the two spectra only if the spectrum is distorted by the intense signal. Indeed, a small distortion is evident in Fig. 9f, which is slightly asymmetric about the Output Y-axis compared with 9b.

6. Conclusions

Equations have been derived which describe the relationship between the phases of the resonator reflection coefficient and both components (absorption and dispersion) of the EPR signal. Phase diagrams based on these equations that are useful for the analysis of the CW EPR signals in spectrometers employing reflection resonators have been presented. By means of these new phase diagrams, techniques to achieve exact tuning to the absorption and dispersion signal in both balanced and unbalanced microwave receivers have been introduced. The presence of additional extraneous signals at the RF input of the microwave receiver (because of the circulator leakage and reflections in the resonator transmission line) has been analyzed. Using both theoretical and experimental phase diagrams, it is shown that setting the receiver output to an extremum as a function of the resonator frequency is necessary and sufficient for the acquisition of the pure absorption signal. This condition is universal: it applies for any spectrometer frequency or configuration. The phase diagrams have illustrated that it is possible to measure the absorption signal with complete suppression of the dispersion signal, independent of the frequency offset between the microwave source and the EPR sample resonator. Finally, equations have been derived that give the approximate relationship between variations of the resonator properties (Q-factor and frequency) and paramagnetic susceptibility.

Appendix A

$$
\begin{aligned}
\Gamma &= \frac{1 - \beta - \mathrm{j}\xi}{1 + \beta - \mathrm{j}\xi} = \frac{1}{1 + \beta} + \frac{1 - \beta - \mathrm{j}\xi}{1 + \beta - \mathrm{j}\xi} - \frac{1}{1 + \beta} \\
&= \frac{1}{1 + \beta} + \frac{(1 - \beta - \mathrm{j}\xi)(1 + \beta) - (1 + \beta - \mathrm{j}\xi)}{(1 + \beta - \mathrm{j}\xi)(1 + \beta)} \\
&= \frac{1}{1 + \beta} - \frac{\beta}{1 + \beta} \cdot \frac{1 + \beta + \mathrm{j}\xi}{1 + \beta - \mathrm{j}\xi} \\
&= \frac{1}{1 + \beta} - \frac{\beta}{1 + \beta} \cdot \exp\mathrm{j}\left[2\tan^{-1}\left(\frac{\xi}{1 + \beta} \right) \right].
\end{aligned} \tag{A.1}
$$

Appendix B

Phase diagrams of the resonator reflection coefficient (depicted in Fig. 2 and subsequently in Figs. 5–7) are very convenient for the characterization and tuning of reflection resonators. These phase diagrams are similar to Smith Charts, which are well known as a general method for the analysis of transmission lines (see [7, Section 12.9, pp. 395–400]). The Smith Chart is a Phase Chart of the reflection coefficient Γ as function of the normalized impedance represented by $(r + jx)$ such that

$$(r + jx) = \mathrm{Re}\left(\frac{Z_{\mathrm{IN}}}{Z_0}\right) + j\,\mathrm{Im}\left(\frac{Z_{\mathrm{IN}}}{Z_0}\right) \tag{B.1}$$

in which (Z_{IN}/Z_0) is the transmission line load input impedance Z_{IN} normalized to the transmission line characteristic impedance Z_0.

In a Smith Chart, as in the phase diagrams presented here, the abscissa and ordinate are the real and imaginary components of Γ, respectively. The circles of a Smith Chart represent traces of either constant real (r) or imaginary (x) components of the transmission line-normalized load impedance $(r + jx)$ (Eq. (B.1)). For the reflection resonators of interest in this work, r and x are not independent variables. We have defined the Phase Diagram variables β and ξ because they represent actual experimental parameters (coupling parameter and frequency offset, respectively) which exhibit the greatest degree of mutual independence with respect to the tuning of reflection resonators. In addition, these are important parameters which are universally employed for the tuning and characterization of resonators. It is almost always possible to estimate or measure β and ξ during the standard spectrometer tuning process, without using additional equipment, but this is not the case for the parameters represented by r or x. It can be shown by Eqs. (1)–(7) that

$$\{r = 1/\beta;\ x = -\xi/\beta\} \Rightarrow x = -\xi r. \tag{B.2}$$

Thus, variation of ξ causes variation of x only, but variation of β causes variation of both r and x. Therefore r and x are mutually dependent parameters if β and ξ are mutually independent, which is the case for most resonator designs.

Appendix C. Relationship between paramagnetic susceptibility and changes of the resonator frequency and Q-factor

Expressions for changes of the resonator complex frequency $\Delta\omega_0$ can be obtained from Maxwell's equations using perturbation theory if $\Delta\omega_0 \ll \omega_0$, which is the normal condition for the acquisition of undistorted EPR spectra.[9,10] The following derivation is achieved using three basic approximations with respect to the interior of the resonator: (1) the dielectric permittivity ϵ is homogeneous and constant; (2) the magnetic permeability μ is homogeneous and constant except for the small change $\Delta\mu \ll \mu$ originating in the sample at resonance from the paramagnetic susceptibility $\chi = \chi' - j\chi''$; (3) the configuration of the microwave field is constant and independent of the EPR paramagnetic susceptibility. Eqs. (C.1a)–(C.1f) are transformations for the determination of a resonator resonant frequency, using these approximations:

$$\begin{aligned}\nabla \times \mathbf{H}_1 &= j\varepsilon\omega_0 \mathbf{E}_1,\\ \nabla \times \mathbf{E}_1 &= -j\mu\omega_0\,\mathbf{H}_1,\end{aligned} \tag{C.1a}$$

$$\begin{aligned}\nabla \times (\nabla \times \mathbf{H}_1) &= j\varepsilon\omega_0 \nabla \times \mathbf{E}_1,\\ \varepsilon\mu\omega_0^2\mathbf{H}_1 &= j\varepsilon\omega_0\,\nabla \times \mathbf{E}_1,\end{aligned} \tag{C.1b}$$

$$\nabla \times (\nabla \times \mathbf{H}_1) = \varepsilon\mu\omega_0^2\mathbf{H}_1, \tag{C.1c}$$

$$\mathbf{H}_1^* \cdot [\nabla \times (\nabla \times \mathbf{H}_1)] = \varepsilon\mu\omega_0^2\mathbf{H}_1^* \cdot \mathbf{H}_1, \tag{C.1d}$$

$$\begin{aligned}&\int_{\mathrm{Resonator}} \mathbf{H}_1^* \cdot [\nabla \times (\nabla \times \mathbf{H}_1)]\,\mathrm{d}V\\ &= \omega_0^2\varepsilon \int_{\mathrm{Resonator}} \mu\mathbf{H}_1^* \cdot \mathbf{H}_1\,\mathrm{d}V,\end{aligned} \tag{C.1e}$$

$$\omega_0^2 = \frac{\int_{\mathrm{Resonator}} \mathbf{H}_1^* \cdot [\nabla \times (\nabla \times \mathbf{H}_1)]\,\mathrm{d}V}{\varepsilon \int_{\mathrm{Resonator}} \mu\mathbf{H}_1^* \cdot \mathbf{H}_1\,\mathrm{d}V}, \tag{C.1f}$$

$\mathbf{H}_1$ and $\mathbf{E}_1$ are amplitudes of the microwave magnetic and electric fields, respectively, and $\mathrm{d}V$ is the resonator volume differential. The slight magnetic permeability change $\Delta\mu$ produces the resonant frequency change $\Delta\omega_0$ and the microwave field variation from $\mathbf{H}_1$ to $\mathbf{H}_1' = a\mathbf{H}_1$. Here a is a scalar constant in accordance with the constant field configuration, as specified by approximation (3) above. This leads to the expression:

$$\begin{aligned}(\omega_0 + \Delta\omega_0)^2 &= \frac{\int_{\mathrm{Resonator}} \mathbf{H}_1'^* \cdot \left[\nabla \times \left(\nabla \times \mathbf{H}_1'\right)\right]\,\mathrm{d}V}{\varepsilon \int_{\mathrm{Resonator}} (\mu + \Delta\mu)\mathbf{H}_1'^* \cdot \mathbf{H}_1'\,\mathrm{d}V}\\ &= \frac{\int_{\mathrm{Resonator}} \mathbf{H}_1^* \cdot [\nabla \times (\nabla \times \mathbf{H}_1)]\,\mathrm{d}V}{\varepsilon \int_{\mathrm{Resonator}} (\mu + \Delta\mu)\mathbf{H}_1^* \cdot \mathbf{H}_1\,\mathrm{d}V},\end{aligned} \tag{C.2}$$

in which μ equals the free space magnetic permeability μ_0 because an EPR resonator is assumed not to contain any magnetic materials except the EPR sample. $\Delta\mu = 0$ outside the EPR sample and inside it $\Delta\mu = \mu_0\chi = \mu_0 (\chi' - j\chi'')$, therefore

$$\begin{aligned}&(\omega_0 + \Delta\omega_0)^2\\ &= \frac{\int_{\mathrm{Resonator}} \mathbf{H}_1^* \cdot [\nabla \times (\nabla \times \mathbf{H}_1)]\,\mathrm{d}V}{\varepsilon\mu_0 \int_{\mathrm{Resonator}} \mathbf{H}_1^* \cdot \mathbf{H}_1\,\mathrm{d}V + \varepsilon\mu_0 \int_{\mathrm{Sample}} \chi\mathbf{H}_1^* \cdot \mathbf{H}_1\,\mathrm{d}V}.\end{aligned} \tag{C.3}$$

The EPR condition creates the resonant complex susceptibility $\chi = (\chi' - j\chi'')$ for those components of the microwave field $\mathbf{H}_1$ which are orthogonal to the static magnetic field $\mathbf{H}_0$. Therefore the field $\mathbf{H}_1$ in Eq. (C.3) can be written for the EPR sample space in term of its EPR-active components $\mathbf{H}_1 \sin \phi$, where ϕ is angle between $\mathbf{H}_1$ and $\mathbf{H}_0$. Substitution of $\mathbf{H}_1 \sin \phi$ into Eq. (C.3) for $\mathbf{H}_1$ together with the assumption of the EPR homogeneous susceptibility χ gives:

$$(\omega_0 + \Delta\omega_0)^2$$

$$= \frac{\int_{\text{Resonator}} \mathbf{H}_1^* \cdot [\nabla \times (\nabla \times \mathbf{H}_1)]\, dV}{\varepsilon\mu_0 \int_{\text{Resonator}} \mathbf{H}_1^* \cdot \mathbf{H}_1\, dV + \varepsilon\mu_0 \chi \int_{\text{Sample}} \mathbf{H}_1^* \cdot \mathbf{H}_1 \sin^2 \phi\, dV}$$

$$= \omega_0^2 \frac{1}{1 + \chi\eta}; \tag{C.4}$$

where

$$\eta = \frac{\int_{\text{Sample}} \mathbf{H}_1^* \cdot \mathbf{H}_1 \sin^2 \phi\, dV}{\int_{\text{Resonator}} \mathbf{H}_1^* \cdot \mathbf{H}_1\, dV}$$

is the filling factor, as defined in Eq. (15). $|\chi\eta| \ll 1$ because $\Delta\omega_0 \ll \omega_0$ was considered above, therefore Eq. (C.4) becomes:

$$\frac{\Delta\omega_0}{\omega_0} = \frac{\Delta\omega_{0\text{Re}} + j\Delta\omega_{0\text{Im}}}{\omega_0} \approx -\frac{1}{2}(\chi' - j\chi'')\eta, \tag{C.5}$$

where $\Delta\omega_{0\text{Re}}$ and $\Delta\omega_{0\text{Im}}$ are equal to the real and imaginary components, respectively, of the resonator frequency complex change $\Delta\omega_0$. The real component $\Delta\omega_{0\text{Re}}$ is the variation of the resonant frequency of the EPR sample resonator. The imaginary component $\Delta\omega_{0\text{Im}}$ is the decrease of the EPR sample resonator unloaded Q-factor. A more accurate derivation which allows for inhomogeneity in the dielectric permittivity and small distortion of the microwave field configuration at resonance leads to the same expression (C.5) but is beyond the scope of this paper [10].

It is possible to convert the imaginary frequency component $\omega_{0\text{Im}}$ to Q-factor by means of the fundamental definition of Q-factor, the relations between loaded and unloaded Q-factors (Q_L and Q_U, respectively), and the radiation Q-factor $Q_R : Q_L^{-1} = Q_U^{-1} + Q_R^{-1}$) (see Section 2 of this paper):

$$Q_L = 2\pi \frac{W(t)}{W(t) - W(t+T)}$$

$$= 2\pi \frac{W(t)}{W(t) - W(t)\exp(-2\omega_{0\text{Im}}T)}$$

$$= 2\pi \frac{1}{1 - \exp(-2\omega_{0\text{Im}}T)} \approx \frac{\omega_0}{2\omega_{0\text{Im}}}, \tag{C.6}$$

$$\frac{2\omega_{0\text{Im}}}{\omega_0} \approx \frac{1}{Q_L} = \left(\frac{1}{Q_U} + \frac{1}{Q_R}\right), \tag{C.7}$$

and

$$\frac{\Delta\omega_{0\text{Im}}}{\omega_0} \approx \frac{1}{2}\Delta\left(\frac{1}{Q_U} + \frac{1}{Q_R}\right) = \frac{1}{2}\Delta\left(\frac{1}{Q_U}\right)$$

$$= -\frac{\Delta Q_U}{2Q_U^2}, \tag{C.8}$$

in which W is the resonator stored energy, t is time, $T = 2\pi/\omega_0$ is microwave period and $\omega_{0\text{Im}}$ is imaginary component of the resonator angular frequency. Finally we obtain from Eqs. (C.5), (C.8) and (10):

$$\left(\frac{\Delta Q_U}{Q_U} + j\Delta\xi\right) = -Q_U\eta(\chi'' + j\chi'), \tag{14}$$

$\Delta\xi$ is defined as originating only from the resonator frequency change and not from a change of the resonator Q-factor Q_U.

References

[1] G. Feher, Sensitivity considerations in microwave paramagnetic resonance absorption techniques, Bell Syst. Tech. J. 36 (1957) 449–484.

[2] T.H. Wilmshurst, Electron Spin Resonance Spectrometers, Hilger, London, 1967.

[3] R.S. Alger, Electron Paramagnetic Resonance: Techniques and Applications, Interscience Publ., New York, 1968.

[4] C.P. Poole Jr., Electron Spin Resonance: A Comprehensive Treatise on Experimental Techniques, Wiley, New York, 1983.

[5] Ya.S. Lebedev, in: L. Kevan, M.K. Bowman (Eds.), Modern Pulsed and Continuous Wave Electron Spin Resonance, Wiley, New York, 1990, pp. 365–435;
V.I. Krinichnyi, 2-mm Wave Band EPR Spectroscopy of Condensed Systems, CRC Press, Boca Raton, 1995;
"International Expert's Workshop: Present and Future of HFEPR," Appl. Magn. Reson. 16 (1999) 159–308;
J.H. Freed, Annu. Rev. Phys. Chem. 51 (2000) 655–689;
T. Prisner, M. Rohrer, F. MacMillan, Annu. Rev. Phys. Chem. 52 (2001) 279–313.

[6] H.H. Skilling, Electrical Engineering Circuits, Wiley, New York, 1957.

[7] G.G. Skitek, S.V. Marshall, Electromagnetic Concepts and Applications, Prentice-Hall, Englewood Cliffs, 1982.

[8] R.W. Quine, G.R. Eaton, J. Magn. Reson. A 119 (1996) 268–270.

[9] J.C. Slater, Microwave Electronics, Van Nostrand, New York, 1950.

[10] R.A. Waldron, The Theory of Waveguides and Cavities, Maclaren, London, 1967.